Fluid Phase Equilibria 405 (2015) 157–166

Contents lists available at ScienceDirect

Fluid Phase Equilibria

journal homepage: www.elsevier.com/locate/fluid

Equation-of-state modeling of associating-fluids phase equilibria in nanopores

Sugata P. Tan*, Mohammad Piri

Department of Chemical and Petroleum Engineering, University of Wyoming, Laramie, WY 82071, United States

ARTICLE INFO

Article history:
Received 8 May 2015
Received in revised form 22 July 2015
Accepted 23 July 2015
Available online 26 July 2015

Keywords:
Porous mediums
Confined fluids
Capillary condensation
Associating fluids
Nanopores

ABSTRACT

Perturbed-Chain Statistical Associating Fluid Theory (PC-SAFT) is coupled with Young–Laplace equation to investigate and represent phase equilibria for associating fluids in nanopores. Despite of stronger fluid–fluid and fluid–wall interactions, the equation of state was found to perform as well as it did for non-associating fluids in the preceding work (Tan and Piri [1]). When the information obtained for pure substances is applied to mixtures in the same porous mediums, the phase equilibrium is accurately predicted, except for strongly-associating mixtures in polar mediums, for which it requires further studies. The promising results presented in this work complement those for non-associating fluids in the preceding study [1] to develop an effective model toward engineering applications in real settings of confined fluids such as chemical systems encountered in unconventional reservoirs (e.g., shale oil and shale gas).

1. Introduction

The effects of confinement in porous mediums on the phase equilibria of entrapped fluids have been successfully represented using the PC-SAFT equation of state (EOS) coupled with the Laplace equation for some simple gases and *n*-alkanes [1]. The approach takes advantage of the robust statistical associating fluid theory in calculating accurate condensed-phase densities and the simple formulation of the Laplace equation in describing the effects of the fluid interfacial curvature on the pressure of the confined system.

There have been efforts to couple the Laplace equation with other simpler EOS, e.g., that of cubic EOS family, to describe confined fluids, but without validation with actual systems [2]. There are also approaches that apply Kelvin's equation to deal with the effects of the confinement [3,4]. Kelvin's equation is obtained when the Laplace equation is used to describe the condensation of simple confined systems where the gas phase is considered ideal and the condensed phase is assumed incompressible, the conditions of which are not valid for fluids confined in nanosize pores. Some other more rigorous approaches apply additional energy term to an EOS that explicitly accounts for the interaction between fluid molecules and the pore walls, such as that by Travalloni et al. [5–7]. Unfortunately, this approach has not been validated for applications at capillary condensation, thus the phase equilibria of real confined systems.

It is found that the macroscopic formulation of the Laplace equation may still be used for nanoscale pores with some modifications [1]. In principle, with an additional parameter derived from experimental data, the calculated pure-substance properties at capillary condensation (such as critical temperature, critical pore radius, surface tension, condensed-phase equilibrium pressure, and saturated densities) are found to be consistent with experimental data, theoretical models, and molecular simulations. The EOS is also proven to work well with binary mixtures in nanopores, which validates the approach for nanoscale applications [1].

Nevertheless, all substances used in the first part of this work series [1] are non-associating in nature, while associating molecules such as water are frequently present in porous mediums not only in shale oil or shale gas, but also in biological structures, top soils, and other industrial applications. Molecular associations, such as that in water, originate from hydrogen-bonding and/or dipolar type of interactions.

An important issue that exists with associating molecules is their strong interactions with the pore walls while they also strongly associate with one another. For water, these fluid–wall interactions are qualitatively expressed using the so-called philicity or its opposite phobicity. If the pore wall "likes" water, the attractive interaction is hydrophilic, otherwise the interaction is not as strong and it is said to be hydrophobic. However, the boundary of these high and low philicities is not clearly defined.

* Corresponding author at: University of Wyoming, Dept. 3295, 1000 E. University Ave., Laramie, WY 82071-2000, United States.
E-mail address: sptan@uwyo.edu (S.P. Tan).

http://dx.doi.org/10.1016/j.fluid.2015.07.044
0378-3812/

Nomenclature

List of symbols

$\tilde{A}$	dimensionless Helmholtz energy
a_{ij}	binary parameter for the surface tension of mixtures Eq. (5)
b_{jk}	coefficients in Eq. (3) for λ parameter
c_{ij}	binary parameter for the surface tension of mixtures Eq. (5)
k_B	Boltzmann constant ($J\,K^{-1}\,molecule^{-1}$)
k_{ij}	binary interaction parameter
m	segment number parameter
P	pressure (bar = 10^{-1} MPa)
$\wp$	parachor ($dn^{1}cm^{11}/mol$)
R	gas constant ($J\,K^{-1}\,mol^{-1}$)
r_p	pore radius (nm)
T	temperature (K)
$\mathbf{x} = \{x_i\}$	mole fractions in adsorbed phases
$\mathbf{y} = \{y_i\}$	mole fractions in the bulk vapor phase

Greek letters

ε_i	LJ energy depth; segment energy parameter of component i (k_B K)
ε_{ik}^{DA}	association energy parameter between site D in a molecule of component i and site A in a molecule of component k (k_B K)
γ	surface tension (dn/cm = mN/m)
κ_{ik}^{DA}	association volume parameter between site D in a molecule of component i and site A in a molecule of component k
λ	parameter
ρ	molar density (mol/cm^3)
σ_i	segment diameter parameter of component i (Å)

Subscripts/superscripts

A	proton-acceptor type of association site
assoc	association
C	critical
cap	capillary
chain	chain
D	proton-donor type of association site
disp	dispersion
hs	hard sphere
i, j	of component i, j
ij	between component i and j
L	of the condensed phase (liquid)
p	pore
res	residual
sat	saturated
V	of the vapor phase (in the bulk)

Abbreviation

EOS	equation of state
PC-SAFT	Perturbed-Chain Statistical Associating Fluid Theory
VLE	vapor–liquid equilibria

For example, MCM-41 silica is considered hydrophilic, and thus can imbibe water spontaneously under ambient pressure [8], but at the same time it is classified as hydrophobic material as it adsorbs more organics than water [9]. Some researchers even consider that water does not wet the MCM-41 inner surface [10], while the others render MCM-41 hydrophilic due to the silanol groups covering the silica surfaces that were revealed by infrared spectroscopy [11]. For discussions on the definition and ambiguity of hydrophobicity of nanoporous materials, the readers are referred to a comprehensive review paper [9]. However, as it happens with any types of fluids in pores, the exact nature of the interactions between the solid walls and the fluid molecules is unknown.

To understand the different behavior between non-associating fluids and their associating counterparts, Fig. 1 shows the experimental capillary-condensation pressure of some associating fluids (water [12,13], ethanol [14,15], and acetone [15]) compared to that of non-associating fluids (N_2 [16], CO_2 [17] and argon [17]). Pressures and temperatures are scaled using bulk properties, i.e., the saturated pressure P_0 and the critical temperature T_C. While the data of water, ethanol, and acetone in porous plates [13,15] were directly measured, the other data were derived from adsorption isotherms where the condensation pressures were estimated when the isotherms undergo abrupt change [1]. This estimation procedure may introduce some uncertainties but they are insufficient to cause ambiguity in interpreting Fig. 1 because MCM-41 and SBA-15 have pores with uniform size and simple geometrical shape, which in turn give a narrow range of condensation pressure on the adsorption isotherms [1].

As shown in Fig. 1, associating fluids condense at relative pressures higher than those of the non-associating fluids in MCM-41 with small pore sizes. In this case, one may deduce that water molecules associate the strongest; in other words, the fluid–wall interaction for water is weakest among the others.

On the other hand, at much larger pore sizes, the associating fluids apparently condense at relative pressures much lower than the non-associating nitrogen does, which means that the fluid–wall interaction for associating fluid molecules is stronger. This behavior is evident from associating fluids in stainless steel and carbon plates, which have pore radii of 6.75 μm and 15 μm, respectively. Despite the much larger sizes, their capillary-condensation pressures are of the same order of magnitudes as that of nitrogen in SBA-15 with a radius of 18 nm. In this case, the fluid–wall interaction for water is apparently strongest, followed in order by ethanol, acetone, and nitrogen. At this point, it can be

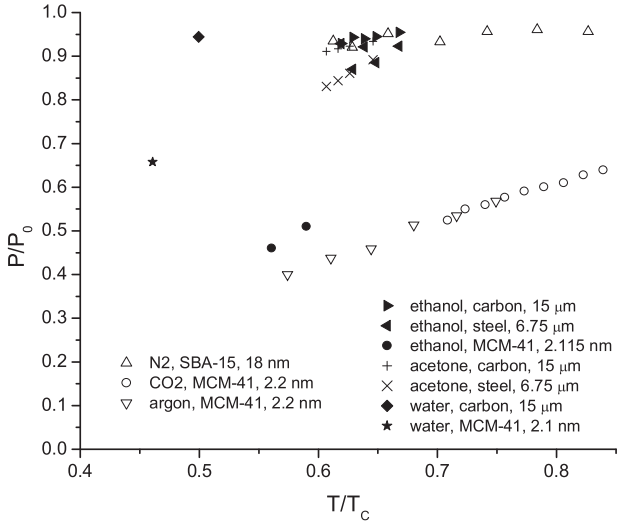

Fig. 1. Capillary condensation of associating molecules compared to that of non-associating molecules. Experimental data: water in MCM-41 [12]; water in carbon plate [13]; ethanol in MCM-41 [14]; ethanol and acetone in steel and carbon plates [15]; N_2 [16]; CO_2 and argon 17]. The numbers next to the porous mediums are the pore radii.

deduced that the behavior of associating fluids shifts from strong fluid–wall interaction at large pores to weaker strength at smaller pores. This distinct feature warrants the current study, as a continuation of that for non-associating fluids [1], toward a complete model of confined-fluid phase equilibria.

Prior knowledge of fluid–wall interactions is not necessary in the EOS presented in this work, which represents the interactions using Laplace equation with an additional parameter as described later. The EOS simply needs the association interaction to be added in the free-energy calculation. Therefore, in this paper it is intended to extend the PC-SAFT/Laplace EOS to account for the association energy, and then to confirm the validity of the approach that has been successfully used with non-associating fluids. Moreover, the inclusion of associating substances other than water in this work will extend the approach to industrial applications such as molecular sieves used for purification.

In the next section, the description of all equations needed to handle confined-fluid phase equilibrium is given, followed by the description of capillary condensation data that are used in deriving the extra parameter needed due to confinement. In Section 3, the modeling results for pure substance and binary mixtures are presented. Properties of pure fluids in porous mediums are discussed within the model, which include critical pore radius, condensed-phase equilibrium pressure, and the saturated phase densities. The critical temperature is not discussed because the temperature range of interest is far below the bulk-phase critical temperature, which is very high for associating molecules (e.g., 647 K for water). The model predictions on the confined-fluid phase behavior of binary mixtures are then discussed and followed by the conclusions.

2. Methods and data

2.1. Phase-equilibrium calculations

The equations for the phase-equilibrium calculations used in this work are mostly the same as those described in our previous paper. It must be underlined here that our EOS does not handle the adsorption process prior to condensation. For more details, the readers are referred to the reference [1].

The difference between phase-equilibria calculations in confined space and those in the bulk-phase cases is that the phases in equilibrium have different pressures (P^{L} in the condensed phase in the pores and P^{V} in the bulk vapor phase). As before, the capillary pressure, P_{cap}, which is the difference between the two pressures across the phase boundary, is given by the Laplace equation for cylindrical pores:

$$P_{\mathrm{cap}}(T,\mathbf{x},\mathbf{y},r_{\mathrm{p}}) = P^{\mathrm{V}} - P^{\mathrm{L}} = \frac{2\gamma_{\mathrm{mix}}(T,\mathbf{x},\mathbf{y},r_{\mathrm{p}})}{r_{\mathrm{p}}(1-\lambda_{\mathrm{mix}}(T,\mathbf{x},r_{\mathrm{p}}))} \tag{1}$$

where T is the system temperature and r_{p} is the physical pore average radius, which can be acquired from pore characterization. The mole fractions in the condensed phase and vapor phase are $\mathbf{x}=\{x_i\}$ and $\mathbf{y}=\{y_i\}$, respectively. The mixture parameter λ_{mix} is obtained from a simple mixing rule applied to those of the pure components:

$$\lambda_{\mathrm{mix}}(T,\mathbf{x},r_{\mathrm{p}}) = \sum_i x_i\lambda_i(T,r_{\mathrm{p}}) \tag{2}$$

The individual λ_i describes how the fluid of component i interacts with the pore wall of a particular material and is derived from the capillary-condensation data. From our previous work, it is correlated in terms of temperature and the pore size [1]:

$$\lambda_i(T,r_{\mathrm{p}}) = \sum_{j=0}\sum_{k=0} b_{jki}T^j r_{\mathrm{p}}^{k-1} \tag{3}$$

where b_{jki} is obtained from the correlation. This parameter is to absorb the strong fluid–wall interaction in pores that induces adsorption of multiple layers of fluid on the wall, which reduces the effective size of the pores [18]. This idea gives the mixing rule Eq. (2) if the adsorbed layer is assumed to be an ideal solution, i.e., the molar volume of the adsorbed solution is a linear combination of the fractional molar volumes of its individual components.

The only property that has to be calculated using a method different from that used for non-associating fluid molecules is the mixture surface tension. The reason for using a different method is that the parachor mixing rule does not work for associating fluids, particularly for aqueous solutions. Therefore, we change the mixing rule to that applicable to any chemical solutions:

$$\gamma_{\mathrm{mix}}(T,\mathbf{x},\mathbf{y},r_{\mathrm{p}}) = \sum_i x_i\gamma_i(T,\mathbf{x},\mathbf{y},r_{\mathrm{p}}) + \Delta\gamma(T,\mathbf{x}) \tag{4}$$

The equation gives the surface tension of the mixture γ_{mix} as the molar average of that of the individual components γ_i plus a deviation due to non-ideality. The most accurate form of the deviation is given by Chunxi et al. [19]:

$$\Delta\gamma = -RT\sum_i\left(x_i\frac{\sum_j x_j c_{ij}\exp(-a_{ij}/T)}{\sum_j x_j\exp(-a_{ij}/T)}\right) \tag{5}$$

where all summations are over the mixture components. R is the gas constant. The binary parameters a_{ij} and c_{ij} are derived from experimental data in the bulk phase and have the following properties:

$$\begin{aligned} a_{ji} &= -a_{ij} \\ c_{ji} &= -c_{ij} \end{aligned} \tag{6}$$

The surface tensions of the individual components in Eq. (4) can still be calculated using the parachor equation [20]:

$$\gamma_i(T,\mathbf{x},\mathbf{y},r_{\mathrm{p}}) = \left[\wp_i(\rho_i^{\mathrm{L}} - \rho_i^{\mathrm{V}})\right]^4 \tag{7}$$

but now with the densities ρ^{L} and ρ^{V}, which are the density of the condensed phase in the pores and the density of the vapor phase in the bulk, respectively, of pure component i at the same temperature as the mixture. As explained in the previous paper,

Table 1
PC-SAFT parameters[a] and the parachor[b] of associating substances.

Substance	m	σ [Å]	$\varepsilon/k_{\mathrm{B}}$ [K][c]	(S^{D},S^{A})	$\varepsilon^{\mathrm{DA}}/k_{\mathrm{B}}$ [K]	κ^{DA}	$\wp$[dn$^{1/4}$ cm$^{11/4}$/mol]
Ethanol	3.1008	2.89558	185.4835	(1,1.25)	2214.460	0.063615	119.6054 + 0.02475T
Acetone	3.4375	2.98768	170.5991	(1,1)	1022.284	1.609174	156.8436 + 0.01907T

[a] D = proton donor; A = proton acceptor.
[b] The parachor is fitted to experimental data in the bulk through Eq. (7) using bulk densities; for water: $\wp = 91.7714 - 0.3517T + 1.176\times10^{-3}\ T^2 - 1.7636\times10^{-6}\ T^3 + 1.0023\times10^{-9}\ T^4$.
[c] k_{B} is the Boltzmann constant.

Table 2
The binary parameters.

Binary mixture	a_{ij}	c_{ij}	k_{ij}
Ethanol + water	−106.698 + 3.526 T (293–323 K)	8.7827–0.01002 T (293–323 K)	$-0.1752 + 7.3208 \times 10^{-4}$ T–9.2234×10^{-7} T^2
Acetone + ethanol	335.251 (at 293 K)	−0.094986 (at 293 K)	$0.1065 - 2.0245 \times 10^{-4}$ T

the dependence on the pore radius r_p is through the calculation of the condensed-phase density in the pores ρ^L that has to be carried out at the pressure P^L. The application of the density in the pores in Eq. (7), instead of that in the bulk, is to account for the effects of the surface curvature on the surface tension of confined fluids [1].

In this work, the parachor in Eq. (7) and the parameters Eq. (6) are generally made temperature-dependent by fitting to the experimental data in the bulk phase to ensure that we can eliminate inaccuracies that may come from the calculation of surface tension so that the behavior of associating fluids in confined space can then be evaluated solely based on the fluid–wall interaction that is represented by the parameter λ.

The crucial role of condensed-phase density calculation in determining the surface tension and the condensed-phase pressure P^L requires an EOS that provides accurate condensed-phase density to the model, such as PC-SAFT described in the next section.

2.2. PC-SAFT

The PC-SAFT EOS is based on the thermodynamic perturbation theory and calculates the residual Helmholtz energy that consists of terms arising from various molecular interactions in the fluid phase:

$$\tilde{A}^{res}(T,\rho,\mathbf{x}) = \tilde{A}^{hs}(T,\rho,\mathbf{x}) + \tilde{A}^{chain}(T,\rho,\mathbf{x}) + \tilde{A}^{disp}(T,\rho,\mathbf{x}) + \tilde{A}^{assoc}(T,\rho,\mathbf{x}) \quad (8)$$

The superscripts hs, chain, disp, and assoc denote the repulsive hard-sphere, the covalent-bonded chain, the attractive dispersive interactions, and the molecular association, respectively. Interested readers are referred to the original work [21,22] for details. Here, we only include the expression to calculate the association free energy [23] that deserves to be presented for clarity.

$$\tilde{A}^{assoc}(T,\rho,\mathbf{x}) = \sum_{i=1}^{n} x_i \sum_{j=1}^{s} S_i^j \left[\ln X_i^j + \tfrac{1}{2}(1 - X_i^j)\right] \quad (9)$$

where the second summation (j) is over two types of association sites ($s = 2$), i.e., the proton-donor and proton-acceptor types of sites. The number of sites of type j in a molecule of component i is S_i^j, and the fraction of molecules i that are not bonded at site j is X_i^j.

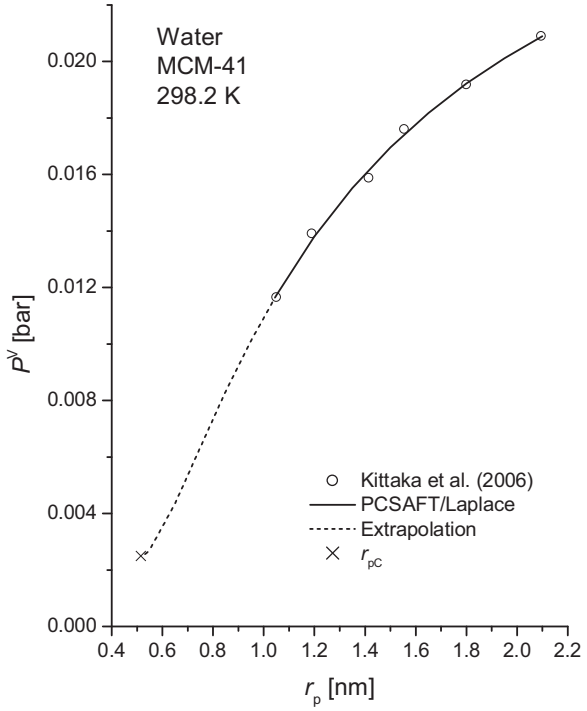

Fig. 2. Capillary-condensation pressures of water in MCM-41 at 298.2 K.

For comprehensive description, the readers are referred to a practical paper that also offers a generalized calculation method of the association energy [23].

As commonly done, we model the water molecule to have two associating sites of proton-donor type (D) and two associating sites of proton-acceptor type (A). The association between molecules, in this case also known as hydrogen bonding, occurs between two sites of different types. The proton-donor sites in water molecules belong to the hydrogen atoms, while the other type belongs to the electron lone-pairs in the oxygen atoms. Such association scheme is known as type 4C. On the other hands, alcohols may be modeled similarly to water, but with more segments representing the alkyl group, which also introduces steric hindrance to one of the

Table 3
Summary of experimental data used in this work.

Fluid	Porous medium	Temperature (K)	r_p (nm)	Reference	Fitted parameter λ
Water	MCM-41	298.2	1.05–2.10	[12]	$-0.38373 + 0.55108/r_p$
	Carbon	323.15	15,000	[13]	0.998841
Ethanol	MCM-41	273.15–303.15	1.32–2.12	[14]	$(-0.592265 + 0.003796\ T) + (0.767666 - 0.002828\ T)\ r_p$
	Carbon	318.15–343.15	15,000	[15]	0.999032
	Steel	318.15–343.15	6750	[15]	$0.859829 + 8.62485 \times 10^{-4}T - 1.335564 \times 10^{-6}\ T^2$
Acetone	Carbon	308.15–328.15	15,000	[15]	$0.989437 + 6.8823 \times 10^{-5}T - 1.2134 \times 10^{-7}\ T^2$
	Steel	308.15–328.15	6750	[15]	$0.947062 + 3.4656 \times 10^{-4}T - 5.775 \times 10^{-7}\ T^2$
Acetone + ethanol	Carbon	323.15	15,000	[13]	–
	Steel	305.15	6750	[13]	–
Ethanol + water	Carbon	323.15	15,000	[13]	–
	Steel	323.15	6750	[13]	–

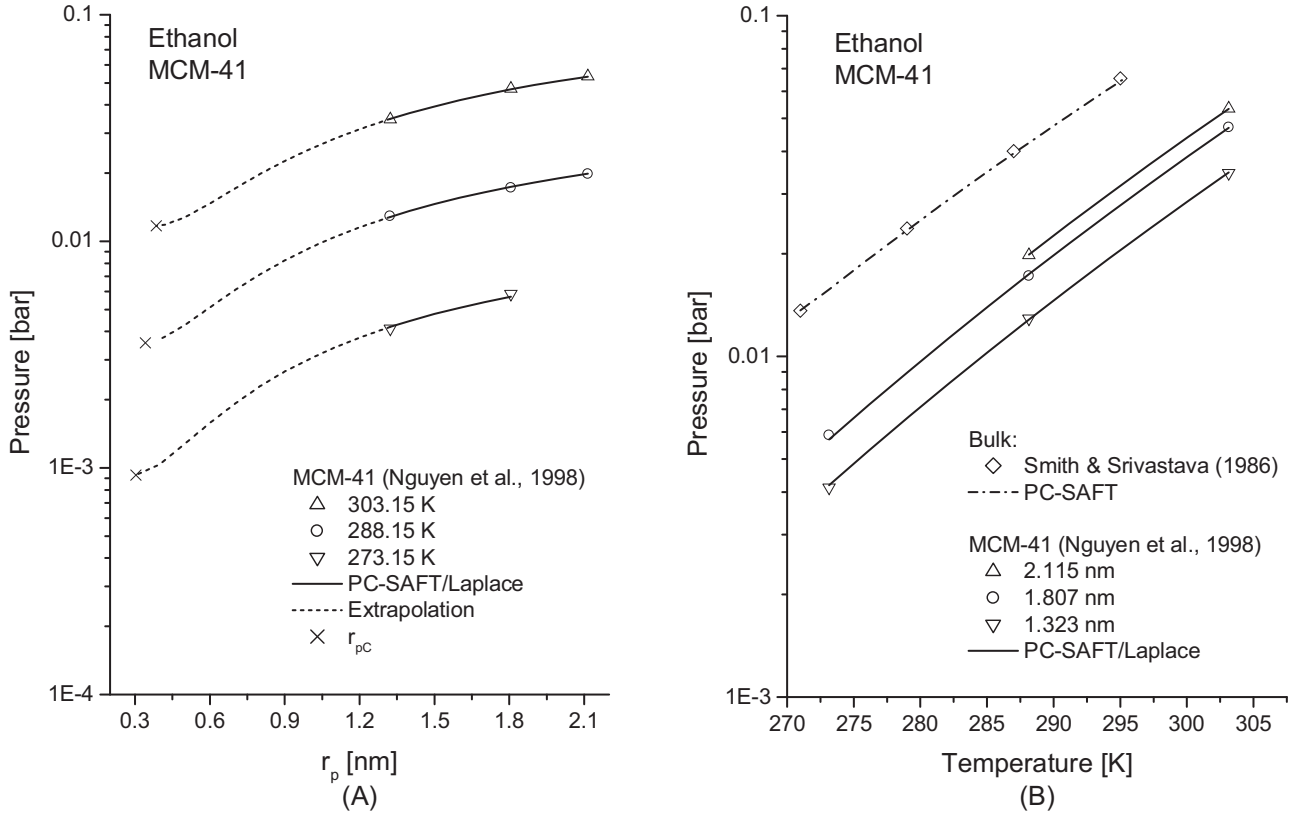

Fig. 3. Capillary-condensation pressures of ethanol in MCM-41: (A) pore-size variations; (B) temperature variations.

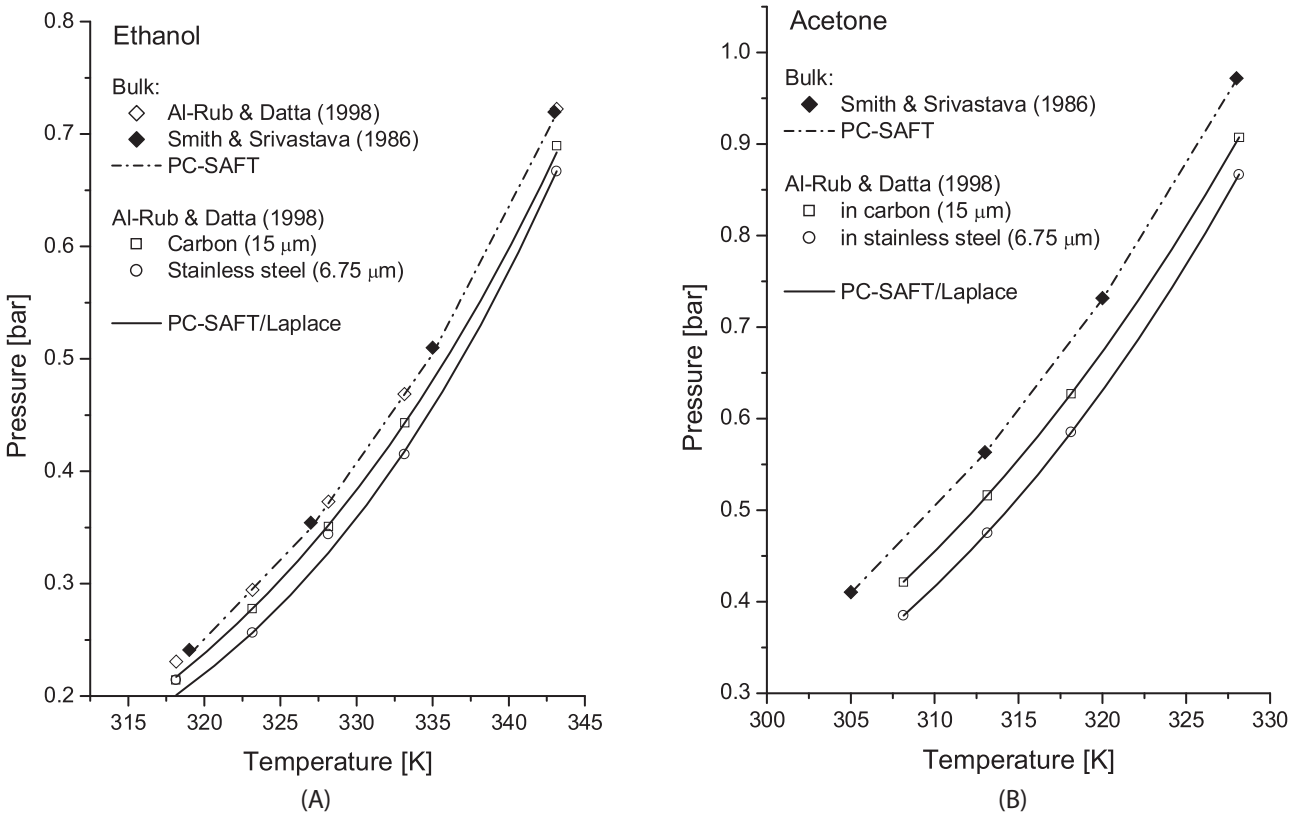

Fig. 4. Capillary-condensation pressures in stainless steel and porous carbon plates: (A) ethanol; (B) acetone.

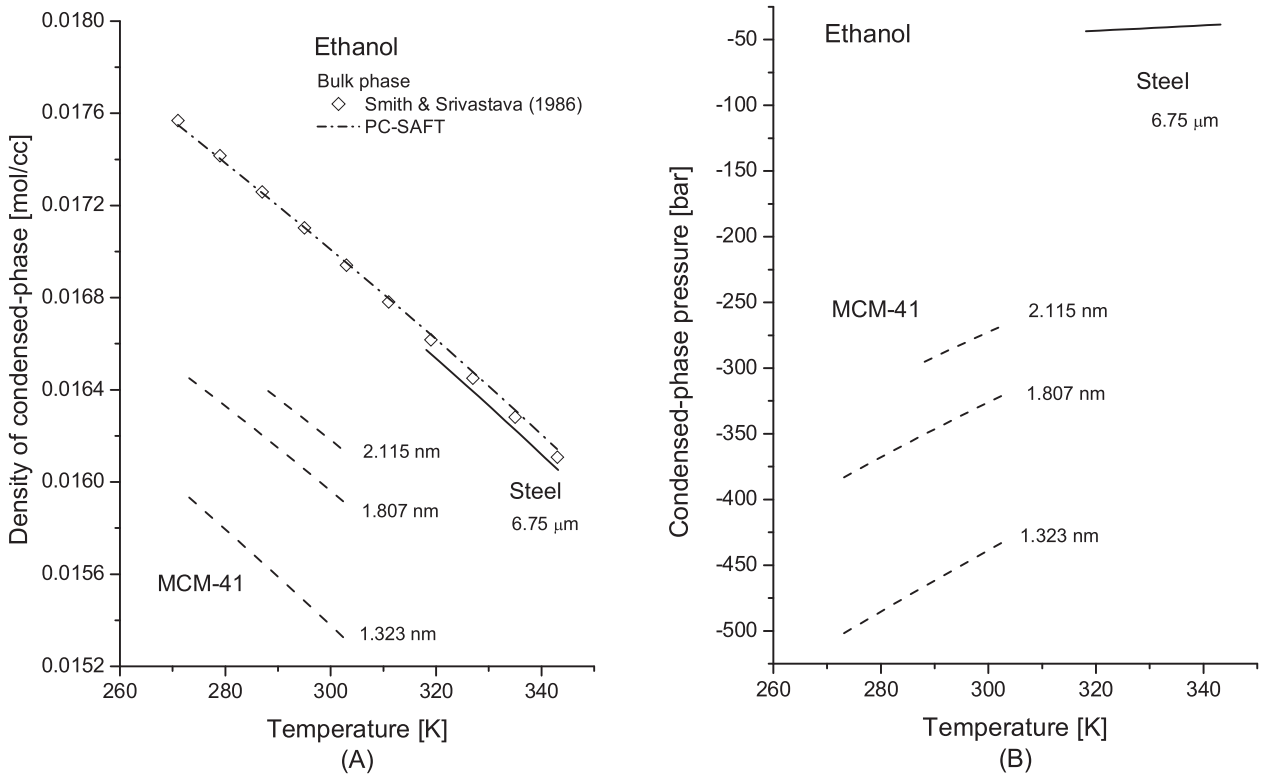

Fig. 5. The behavior of condensed phase in MCM-41 and steel with respect to temperature: (A) saturated density; (B) pressure.

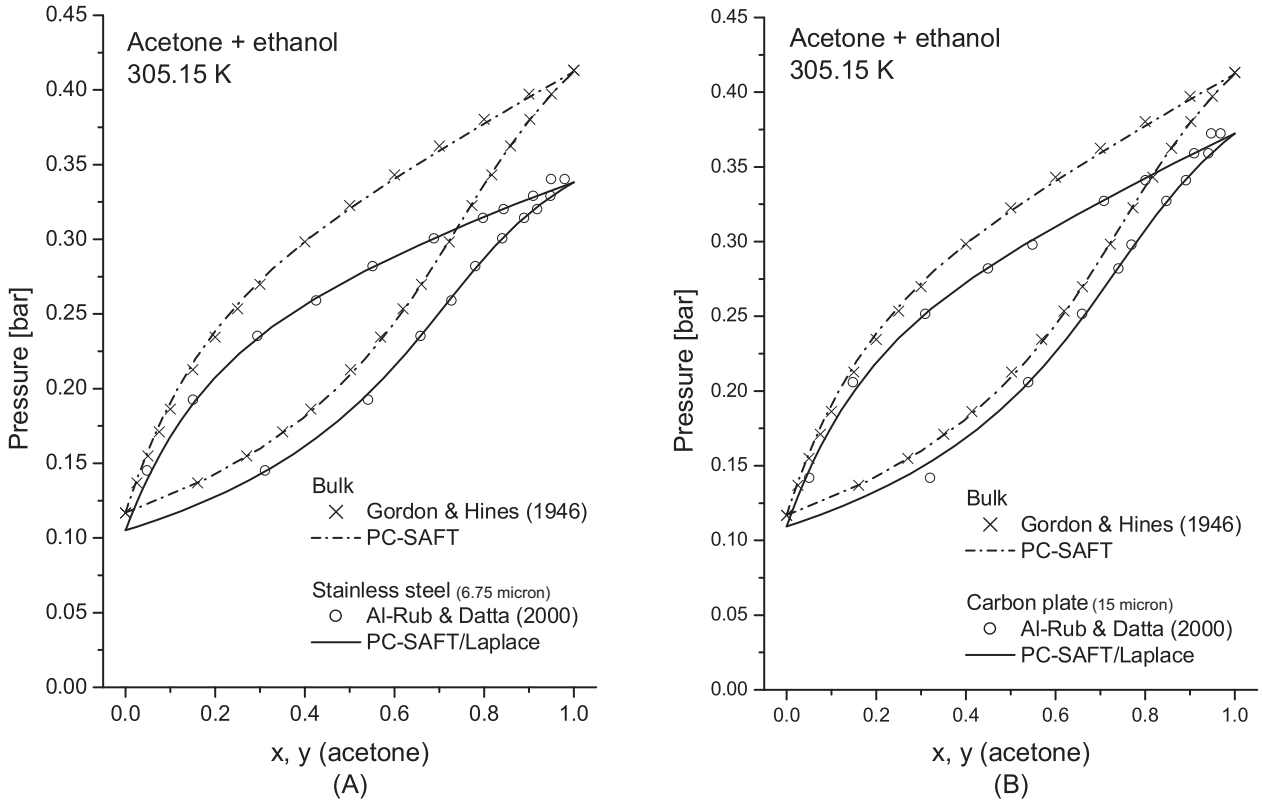

Fig. 6. Prediction of PC-SAFT/Laplace on the VLE of the binary acetone/ethanol in: (A) stainless steel; (B) carbon.

electron lone pairs at the oxygen atom. Therefore, instead of having two full association sites on the oxygen atom, for example, ethanol only has less than two effective sites of proton-acceptor type. For acetone, which has a strong dipole moment, its molecule may be modeled to have one proton-donor and one proton-acceptor association sites ($S^D = S^A = 1$), instead of applying an additional energy term that accounts for polarity in Eq. (8). This simpler approach works accurately as discussed later in the next section.

The EOS parameters of substances discussed in this paper are summarized in Table 1. Parameters for water are taken from the literature [24], except for its parachor, which is given in the footnote below Table 1. The parameters of ethanol and acetone are derived from the saturated vapor pressure and saturated density data of bulk liquid outside the pores, i.e., the data by Smith and Srivastava [25]. They are the segment number m, segment diameter σ, the dispersive potential energy ε, the association energy ε^{DA}, and the association volume κ^{DA}. As a caution note, the parameters in Table 1 were obtained also by matching their performances for binary mixtures. For associating fluids, where many parameter sets may describe the pure-substance properties equally well, it is recommended to select a unique set of parameters that can give satisfactory performance for binary mixtures. In Table 1, the number of association sites of ethanol is $S^D = 1$ and $S^A = 1.25$ (effective number due to steric hindrance), which is necessary to get good representations not only for the pure ethanol, but also the vapor–liquid equilibria (VLE) of binary mixtures containing ethanol as evident in Figs. 6 and 7. References of experimental data and the parameterization are presented in the Supplementary materials that accompanies this paper.

For mixtures, the binary interaction parameter, k_{ij}, is commonly used to fine-tune the interaction between unlike fluid molecules and fitted to experimental VLE data of binary mixtures. It is applied in the cross parameter of the segment energy of the mixtures:

$$\varepsilon_{ij} = \sqrt{\varepsilon_i \varepsilon_j}(1 - k_{ij}) \tag{10}$$

The mixing rules for the association parameters follow [26]:

$$\varepsilon^{DA}_{ki} = \tfrac{1}{2}\left(\varepsilon^{DA}_{kk} + \varepsilon^{DA}_{ii}\right) \tag{11}$$

$$\kappa^{DA}_{ki} = \sqrt{\kappa^{DA}_{kk}\kappa^{DA}_{ii}}\left(\frac{\sqrt{\sigma_k \sigma_i}}{\frac{1}{2}(\sigma_k + \sigma_i)}\right)^3 \tag{12}$$

The binary parameters of the surface tensions a_{ij} and c_{ij} in Eq. (5) are fitted to experimental data and summarized in Table 2 along with the k_{ij} in Eq. (10).

The parameters in the bulk phase in Tables 1 and 2 are then used in the EOS to derive the parameter λ from capillary-condensation data to describe the fluid phase equilibria in confined space.

2.3. Capillary-condensation data

As described in the previous paper [1], the useful experimental data for pure substance are the capillary-condensation pressures (P^V), the values of which may be obtained from adsorption isotherms at condensation. The pressure is analogous to the vapor pressure in unconfined bulk phases. We use P^V data to derive the EOS parameter λ and its correlation in Eq. (3). When possible, experimental data for capillary condensation were taken from systems in well-characterized porous mediums such as MCM-41. The advantage of using such synthetic mediums is the uniform size and simple geometrical shape of the pores, which in turn enables

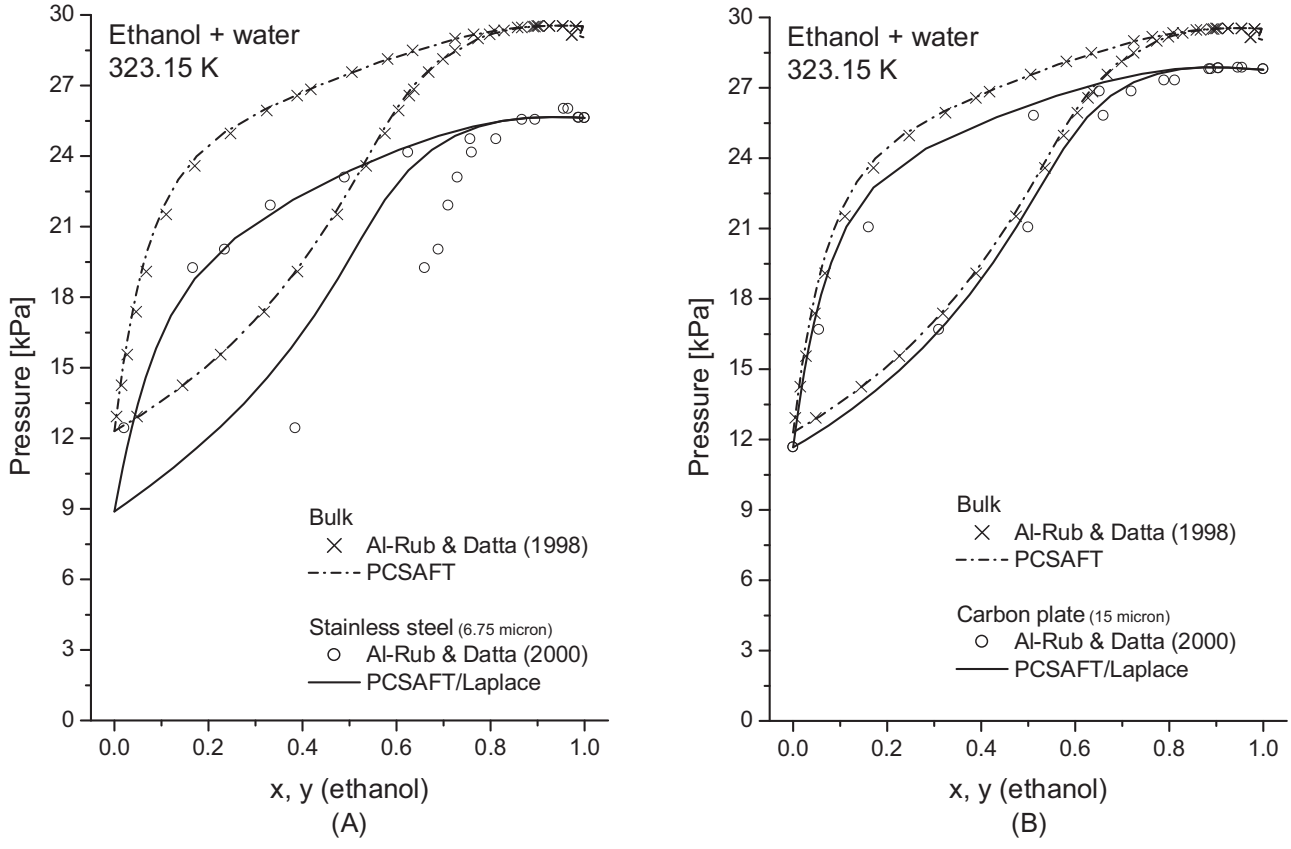

Fig. 7. Prediction of PC-SAFT/Laplace on the VLE of the binary ethanol/water in: (A) stainless steel; (B) carbon.

investigations on important factors that come into play for modeling purposes.

The confined-phase equilibria data for binary mixtures containing associating fluids are almost non-existent. To the best of our knowledge, the only data sets, which are directly in a VLE form, were obtained from investigative work series for capillary distillation using stainless steel (polar medium) and porous carbon (non-polar medium) plates that have micron-size pores [13]. As shown in Fig. 1, despite the large pore sizes, the capillary condensation of the constituting components in these mediums follows the trend seen in nanosize pores containing non-associating fluids, which justifies the data to be used for validation purposes. This statement will be verified later in the discussion. As mentioned before, the fluid–wall interaction of these systems is apparently very strong in larger pores, but relatively weak in nanopores, where the fluid association may be more dominant. This behavior could be due to a strong competition between the association energy of the fluid molecules and the fluid–wall interaction in the confined space.

The experimental data used in this work for pure components and binary mixtures, and their references are listed in Table 3.

3. Results and discussion

3.1. Pure substance

It turns out that the approach that was used for non-associating fluids [1] is applicable for associating fluids, regardless of their host porous mediums. The λ parameters are fitted to the experimental data and summarized in last column of Table 3. Only the data set for ethanol in MCM-41 has variations in terms of temperature and pore sizes, which enables the fitting of λ to the both T and r_p according to Eq. (3).

As listed in Table 3, the parameters λ of systems in steel and carbon all have magnitudes close to 1 in the experimental temperature range. When they are applied to Eq. (1) and interpreted as the reduction of the pore radii, the effective radii are all far below the measured sizes, for example, ethanol in carbon has λ = 0.999032, which leads to an effective radius of 14.52 nm in our EOS. Therefore, despite of their larger pores, the phase behavior of these systems follow that of non-associating fluids in much smaller pores. This fact justifies the use of these data, particularly when the substances are later used as the constituting components of mixtures in the same porous mediums for the EOS validation, considering that mixture data in nanopores are non-existent.

The performance of the EOS for individual systems is shown in the following figures. Water in MCM-41 at 298.2 K is shown in Fig. 2, where the calculation is extrapolated to get the critical pore radius r_{pC} of 0.5153 nm. According to the discussion in our previous paper [1], this also means that the pore critical temperature of water in MCM-41 with 0.5153-nm radius is 298.2 K. Ethanol in MCM-41 is shown in Fig. 3. Extrapolation to critical pore radius finds r_{pC} that is less than 0.4 nm for all temperatures presented in the data set. These small critical pore radii, only a few times larger than the molecular radii, are another evidence for the stronger fluid–wall interactions compared to the case of non-associating fluids, e.g., about 1 nm for nitrogen in SBA-15 at 80 K [1].

Fig. 4 shows the trends for ethanol and acetone in stainless steel and porous carbon plates. In the figure, the bulk-phase vapor pressures are given for comparison. However, comparison between the two porous mediums is hampered by the fact that the polar medium, in this case steel, has the smaller pores. Smaller size of pores and stronger polarity of the pore wall both enhance the effects of the confinement to the fluid inside the pores.

The behavior of saturated condensed-phase densities and the corresponding equilibrium pressures in MCM-41 and steel is

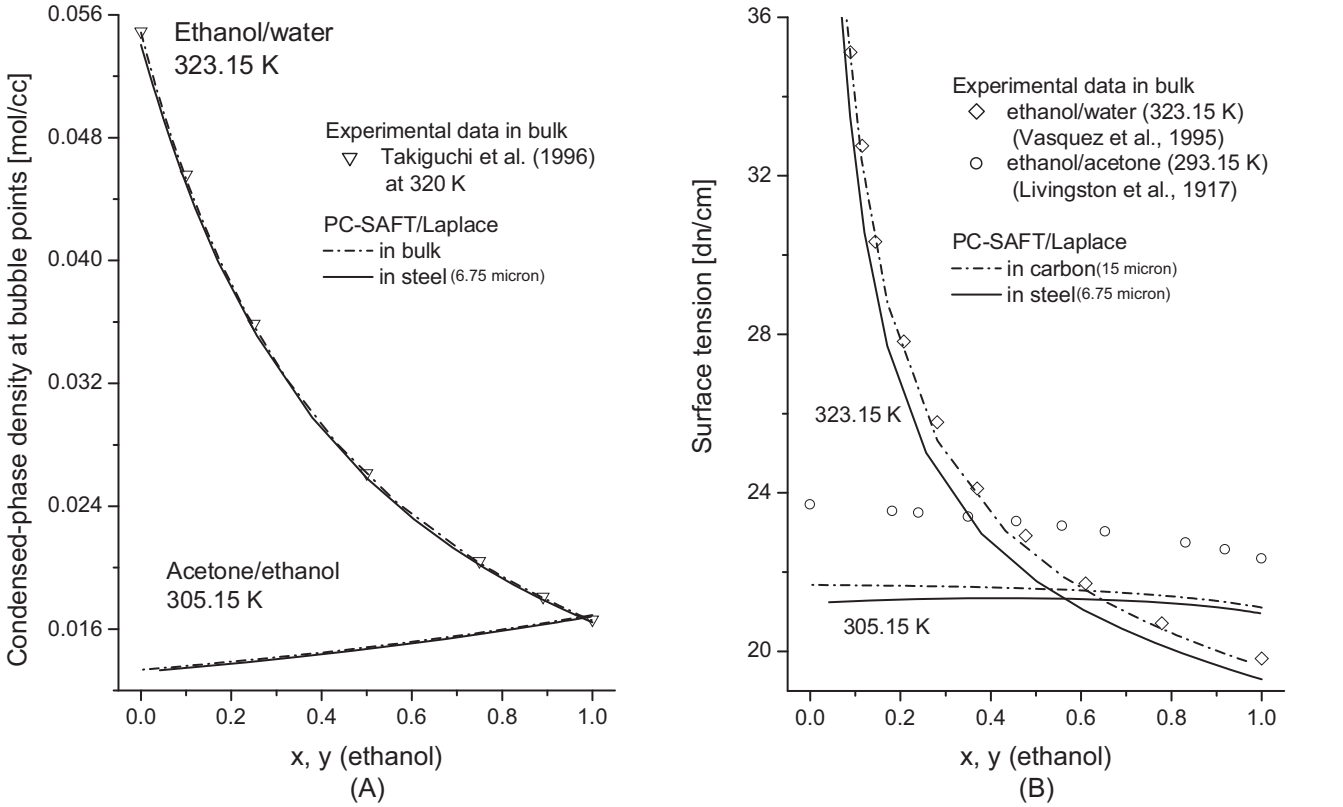

Fig. 8. Properties of the binary mixtures in confined space along the bubble points of the binary: (A) condensed-phase density; (B) surface tension. Experimental data of surface tension in the bulk is given for comparison; note: it is at 293.15 K for ethanol/acetone.

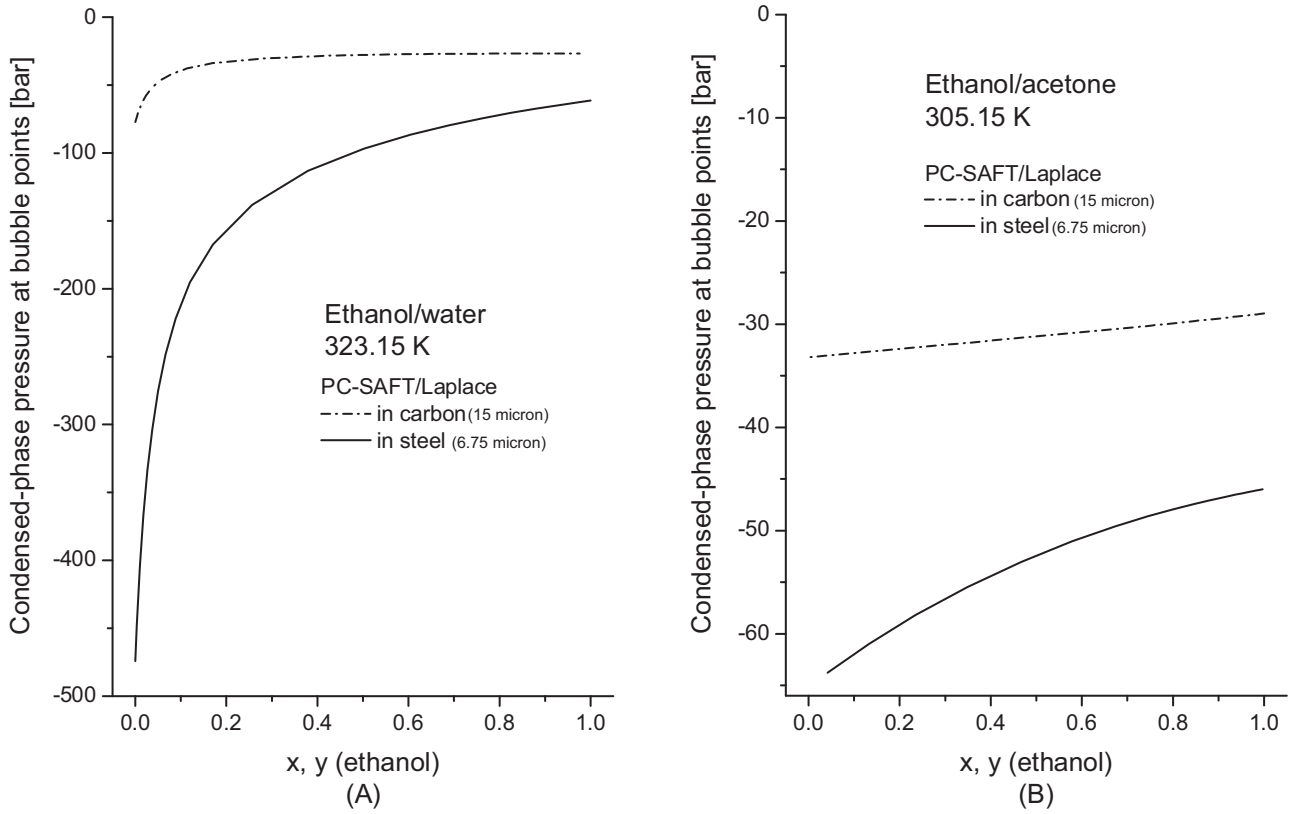

Fig. 9. The tension (negative pressure) in the condensed phase along the bubble points of the binary: (A) ethanol/water; (B) ethanol/acetone.

shown in Fig. 5 for ethanol, which has the most complete set of data. Water and acetone behave similarly. As expected, the smallest pores have the largest confinement effects as evident from the density calculation. Unfortunately, volumetric saturation data is not available to convert the amount of adsorbed fluid (as measured in the adsorption isotherms) into its density, which otherwise can serve as a way to validate the density calculations [1]. However, as Fig. 5A suggests, if the calculations are compared to that of the bulk-phase density and their measured data, they are all found to be consistent with one another. The consistency, which provides correct qualitative behavior, serves as a first approximation towards quantitative validation of the model that can be done when data are measured in the future.

3.2. Binary mixture

As a note, the EOS performances for the binary mixtures in confined space presented here are all prediction, which means no bulk-phase parameters, both of pure substance and their binaries, were adjusted in the calculations. Therefore, the performances serve as the validation of the EOS.

As seen in Fig. 6, the EOS provides excellence description of the binary acetone/ethanol in both polar medium (stainless steel) and non-polar medium (carbon). The performance of the PC-SAFT in the bulk phase along with experimental data [27] is also shown for comparison. While it could not be done with pure fluids in Fig. 4, comparison between Figs. 6A and B reveals that the fluid–wall interaction is stronger in the stainless steel than it is in carbon plate.

However, the prediction does not perform satisfactorily in the case of ethanol/water in stainless steel, as seen in Fig. 7A, though it is still very good for the binary in porous carbon plate in Fig. 7B. Noticeably, the prediction for stainless steel is pretty accurate only for the bubble-point pressures. The prediction of the dew points is far from the experimental measurements. Moreover, as there is no experimental data for pure water in steel that corresponds to that in the binary, the parameter λ of water in steel was correlated directly to the binary data ($\lambda = 0.9996$) to calculate the solid curves in Fig. 7A. For these reasons, there is no point presenting the data sets of this binary at two other temperatures (328.15 K and 333.15 K) from the data source [13].

The deviation of the prediction on the dew points for aqueous ethanol in steel is of unknown origin. As it may be seen from Figs. 6 and 7, the presence of the confining walls generally narrows the two-phase regions in the phase diagrams, where vapor and condensed phases coexist. This feature is consistent with that of pure substance, where the critical point substantially drops in porous mediums. However, a medium with strong polarity, such as stainless steel, seemingly introduces some effects that enlarge the two-phase region when interacting with strongly associating fluids such as ethanol/water, i.e., pushing the dew points to lower pressures. This phenomenon does not occur if the medium is non-polar such as carbon or if the fluids do not associate strongly enough such as acetone/ethanol. The presence of the strongly polar medium may somehow reduce the strength of cross association between water and ethanol molecules, the behavior of which is not accounted for in the current EOS.

In fact, capillary distillations in separation process for strongly associating fluids using polar mediums are meant to benefit from this broadening two-phase region, which ultimately pushes the azeotrope to the side of less polar pure component [28,29]. For example, the azeotrope of the bulk ethanol/water was both calculated and experimentally to be at about 5-mol% of water, as shown in Fig. 7. The azeotrope remains more or less at the same composition in porous carbon in Fig. 7B, while experimentally it is almost gone in stainless steel in Fig. 7A as discussed in the data

source [13]. Because PC-SAFT/Laplace predicts a narrower two-phase region, the azeotrope remains by calculation at about the same composition but at a lower pressure. To investigate this peculiar deviation, additional data with other systems are needed, which establishes a subject of future research.

Our calculations also provide the density, surface tension, and pressure of the condensed phase of the solutions. Even though there are no experimental data to verify the calculations here, the results are found to be consistent if compared to the data and calculation for the properties of the bulk phases. Again, the consistency, which provides correct qualitative behavior, serves as a first approximation to quantitative validation once experimental data are available in the future. Fig. 8 shows the calculated densities and surface tensions along the bubble points, while Fig. 9 describes the condensed-phase pressure. Perhaps, the latter is of greater interest due to its negative values, which refers to tension instead of pressure. This behavior is consistent with that in pure substances, such as ethanol in MCM-41 in Fig. 5B, and described in details in our previous paper [1].

The density and surface tension of the fluids in confined space all decrease with respect to their values in the bulk phase [30–32]; the decrease occurs in stainless steel is greater than that in carbon due to the stronger wall effects in polar mediums such as steel. The stronger interaction by steel is also evident in Fig. 9, where the tension (negative pressure) in the condensed phase is larger. The tension difference between fluids in mediums of different polarity is even more dramatic for strongly associating fluids such as ethanol/water as shown in Fig. 9A.

4. Conclusion and remark

The PC-SAFT/Laplace EOS was shown to work well in describing associating fluids in confined space. The approach in this model is validated as demonstrated for binary mixtures in porous mediums, where presented calculations are all predictions. Upon combining the results of this work with those in the previous work for non-associating fluids [1], the PC-SAFT/Laplace in general provides effective representations of the VLE in confined space, including nanopores, as long as the surface tension is accurately calculated and the pore wall is non-polar. In summary, the approach of PC-SAFT/Laplace gives reliable prediction on the phase properties and behavior of fluid mixtures in non-polar porous mediums, just based on the corresponding bulk-phase behavior and the correlated behavior of the constituting components in the same non-polar pore walls as that of the mixtures.

The representation of dew points for strongly associating fluids in polar mediums, such as ethanol/water in steel, however, still needs further investigation. In such systems, both fluid association and fluid–wall interactions are stronger than in the cases of confined non-associating fluids. The resulting wider two-phase region of the confined binary mixtures may arise from the decreasing cross association of the fluid mixture components due to the presence of the polar pore walls. The need for measuring additional experimental data to investigate this issue would initiate some future research efforts that are beyond the scope of the current work.

Acknowledgments

We gratefully acknowledge financial support of Hess Corporation and the School of Energy Resources at the University of Wyoming.

Appendix A. Supplementary data

Supplementary material associated with this article consists of some supporting figures that show the performance of the EOS in representing the bulk-phase equilibria and surface tension, both for pure substance and binary mixtures. The material can be found in online version, at http://dx.doi.org/10.1016/j.fluid.2015.07.044.

References

[1] S.P. Tan, M. Piri, Fluid Phase Equilib. 393 (2015) 48-63 and the references there in.
[2] B. Nojabaei, R.T. Johns, L. Chu, SPE Res. Eval. Eng. (2013) 281–289.
[3] A.A. Shapiro, E.H. Stenby, Fluid Phase Equilib. 134 (1997) 87–101.
[4] R.J.-M. Pellenq, B. Coasne, R.O. Denoyel, O. Coussy, Langmuir 25 (2009) 1393–1402.
[5] L. Travalloni, M. Castier, F.W. Tavares, S.I. Sandler, Chem. Eng. Sci. 65 (2010) 3088–3099.
[6] L. Travalloni, M. Castier, F.W. Tavares, Fluid Phase Equilib. 362 (2014) 335–341.
[7] K. Dhanapal, D. Devegoda, Y. Zhang, A.C. Contreras-Nino, F. Civa, SPE (2014) 169008-MS.
[8] A. Han, Y. Qiao, J. Phys. D: Appl. Phys. 40 (2007) 5743–5746.
[9] E.-P. Ng, S. Mintova, Microporous Mesoporous Mater. 114 (2008) 1–26.
[10] N. Floquet, J.P. Coulomb, N. Dufau, G. Andre, R. Kahn, Adsorption 11 (2005) 139–144.
[11] S. Gruener, T. Hofmann, D. Wallacher, A.V. Kityk, P. Huber, Phys. Rev. E 79 (2009) 067301.
[12] S. Kittaka, S. Ishimaru, M. Kuranishi, T. Matsuda, T. Yamaguchi, Phys. Chem. Chem. Phys. 8 (2006) 3223–3231.
[13] F.A.A. Al-Rub, R. Datta, Sep. Sci. Technol. 35 (2000) 2203–2225.
[14] C. Nguyen, C.G. Sonwane, S.K. Bhatia, D.D. Do, Langmuir 14 (1998) 4950–4952.
[15] F.A.A. Al-Rub, R. Datta, Fluid Phase Equilib. 147 (1998) 65–83.
[16] K. Morishige, M. Ito, J. Chem. Phys. 117 (2002) 8036–8041.
[17] K. Morishige, Y. Nakamura, Langmuir 20 (2004) 4503–4506.
[18] R. Evans, U.M.B. Marconi, P. Tarazona, J. Chem. Soc. Faraday Trans. 82 (1986) 1763–1787.
[19] L. Chunxi, W. Wenchuan, W. Zihao, Fluid Phase Equilib. 175 (2000) 185–196.
[20] B.E. Poling, J.M. Prausnitz, J.P. O'Connell, The Properties of Gases and Liquids, 5th ed., McGraw-Hill, New York, 2001.
[21] J. Gross, G. Sadowski, Ind. Eng. Chem. Res. 40 (2001) 1244–1260.
[22] J. Gross, G. Sadowski, Ind. Eng. Chem. Res. 41 (2002) 5510–5515.
[23] S.P. Tan, H. Adidharma, M. Radosz, Ind. Eng. Chem. Res. 43 (2004) 203–208.
[24] S.P. Tan, Y. Yao, M. Piri, Ind. Eng. Chem. Res. 52 (2013) 10864–10872.
[25] B.D. Smith, R. Srivastava, Thermodynamic Data for Pure Compounds, Part A and Part B, Elsevier, New York, 1986.
[26] J.P. Wolbach, S.I. Sandler, Ind. Eng. Chem. Res. 37 (1998) 2917–2928.
[27] A.R. Gordon, W.G. Hines, Can. J. Res. 24b (1946) 254–262.
[28] G.C. Yeh, B.V. Yeh, S.T. Schmidt, M.S. Yeh, A.M. McCarthy, W.J. Celenza, Desalination 81 (1991) 161–187.
[29] F.A.A. Al-Rub, J. Akili, R. Datta, Sep. Sci. Technol. 33 (1997) 1529–1550.
[30] Y. Takiguchi, O. Osada, M. Uematsu, J. Chem. Thermodyn. 28 (1996) 1375–1385.
[31] G. Vasquez, E. Alvarez, J.M. Navaza, J. Chem. Eng. Data 40 (1995) 611–614.
[32] J. Livingston, R. Morgan, A.J. Scarlett Jr., J. Am. Chem. Soc. 39 (1917) 2275–2293.